γ-ray spectroscopy of ^{150}Sm through the β decay of ^{150}Pm ($T = 2.7$ h) and ^{150}Eu^m ($T = 12.8$ h)

P. Schmelzenbach
Department of Physics and Engineering, Point Loma Nazarene University, San Diego, California 92106, USA

K. S. Krane
Department of Physics, Oregon State University, Corvallis, Oregon 97331, USA

J. L. Wood and W. D. Kulp
School of Physics, Georgia Institute of Technology, Atlanta, Georgia 30332, USA

J. Loats
Metropolitan State University of Denver, Denver, Colorado 80204, USA

C. J. Staples
The Mathworks Inc., Natick, Massachusetts 01760, USA

E. B. Norman
Department of Nuclear Engineering, University of California, Berkeley, California 94720, USA

(Received 15 June 2018; revised manuscript received 23 August 2018; published 12 September 2018)

The ^{150}Sm nucleus, populated through the β decays of ^{150}Eu^m and ^{150}Pm, was investigated by means of γ-γ coincidence and γ-γ angular correlation studies using an array of 20 Compton-suppressed Ge detectors. The study particularly focuses on the determination of weakly populated levels and weak decay branches between established levels. A weakly populated state at 1603 keV is established to have spin-parity 0^+ from the angular correlation data; a second weakly populated state at 1786 keV is confirmed to have spin-parity 0^+ on a similar basis.

DOI: 10.1103/PhysRevC.98.034311

I. INTRODUCTION

Nuclei far from closed shells can be described in terms of collective behavior. The onset of collective behavior occurs in the region around neutron number $N = 90$, which has been widely studied through experiment and theory [1–6]. In these nuclei, a change of ± 2 in N can result in a sudden change of the nuclear properties. The stable nuclide ^{150}Sm with $N = 88$ lies in this transitional region and is populated in both β^- and β^+ decays from, respectively, ^{150}Pm and ^{150}Eu. (^{150}Sm is also of interest because it is populated in the 2β decay of ^{150}Nd [7,8].) The Q values of the β decays are large (>2 MeV) and so a multitude of states are populated in both decays and the decay schemes are complex (for example, more than 30 levels are populated by more than 130 γ rays in the Pm decay). However, the spectroscopy data on these decays are relatively old, mostly dating from the 1970s and taken with detectors of relatively low efficiency and poor resolution compared with current spectroscopic technology. We have therefore undertaken a new study of the low-spin decays that lead to states in ^{150}Sm using a multidetector array, with particular emphasis on using the γ-ray angular correlations to locate the 0^+ states.

The two different parents used to populate ^{150}Sm through β decay in this study were ^{150}Eu^m ($Q = 2301$ keV, $J = 0^-$, $T_{1/2} = 12.8$ h) and ^{150}Pm ($Q = 3454$ keV, $J = 1^-$, $T_{1/2} = 2.68$ h). Because the two parents have similar spins, but ^{150}Eu^m has a lower Q value, most transitions seen in the ^{150}Eu^m decay were also seen in the ^{150}Pm decay. In this way, the ^{150}Eu^m decay data help confirm placements of many transitions observed in the more complicated decay scheme of ^{150}Pm. In previous experiments, ^{150}Sm was studied through both of these decays [9–11], as well as through Coulomb excitation and particle reactions [12–15]. In the present study, the use of a detector array made it possible to identify weak transitions and unravel a complicated decay scheme with much greater confidence. The present paper provides details of observed γ rays, transition assignments, and level assignments with spin and parity, based on analysis of γ singles, γ-γ coincidences, and γ-γ angular correlations.

II. EXPERIMENTAL DETAILS

Both ^{150}Pm and ^{150}Eu^m were produced at the 88-inch cyclotron located at Lawrence Berkeley National Laboratory. The Pm was produced by bombarding enriched neodymium oxide (97.84% mass 150) with 10 MeV protons in the ^{150}Nd$(p,n)^{150}$Pm reaction. The product was apportioned so that each of nine samples was counted starting with an activity

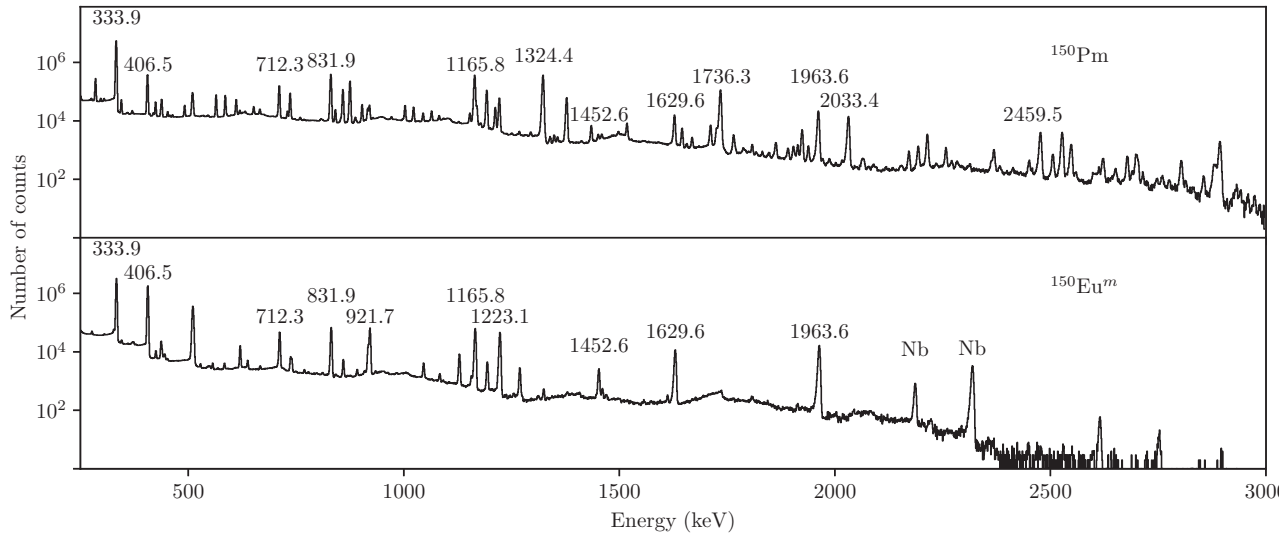

FIG. 1. Scaled down γ-ray singles spectra from ^{150}Pm and ^{150}Eu^{m}. The ^{150}Eu^{m} source had several weak impurities, the strongest of which is ^{90}Nb.

of 10 μCi. Each sample was counted for approximately one half-life, for a total counting time of 24.8 h and a total of 3.4×10^7 coincidence events. Singles events were simultaneously measured in a scaled-down mode, with a total of 5.5×10^7 counts recorded.

In a similar fashion, ^{150}Eu^{m} was produced by bombarding enriched samarium oxide (99.93% mass 150) with 10 MeV protons in the ^{150}Sm$(p,n)^{150}$Eu^{m} reaction. The product was divided so that three samples initially 10 μCi were counted for around one half-life, for a total of counting time of 26.6 h. A total of 5.3×10^7 coincidence events and 4.3×10^7 scaled-down singles counts were recorded.

Both singles and coincidence measurements were made using the 8π spectrometer [16]. This detector array consists of 20 Compton-suppressed high-purity germanium (HPGe) detectors located 22 cm from the source in these measurements. These detectors differed slightly in their crystal sizes, which ranged between 109 and 127 cm^3. In the geometry of the 20 detectors, only five unique angles exist between all 190 possible detector pairs. These angles of 41.8°, 70.5°, 109.5°, 138.2°, and 180° occur in the ratio of 3:6:6:3:1. This arrangement of detectors was designed to reduce the effect of angular correlations in the combined coincidence data. Of note, while achieving its original purpose of reducing angular correlation effects when combining all coincidence data, the detector array allows for excellent angular correlation measurements when using subsets of the detectors. Because only a few angles exist, high statistics were collected at each of these angles. This, in combination with Compton suppression, allowed for determination of angular correlation coefficients and measurements of weak transitions.

III. RESULTS

Singles and γ-γ coincidence analysis was accomplished using RADWARE [17]. Singles counts were collected in a scaled-down mode, allowing for a greater coincidence count rate. The singles spectrum for each decay is shown in Fig. 1. The ^{150}Eu^{m} source had several weak impurities, the strongest being ^{90}Nb.

The energy calibration in ^{150}Eu^{m} was constructed utilizing the ^{90}Nb and other weak impurities in the samples. The ^{150}Pm samples were relatively free of impurities and the energy calibration was made using strong transitions also seen in the ^{150}Eu^{m} in conjunction with data from the Nuclear Data Sheets [18]. An efficiency calibration for individual detectors, as well as the detector array, was determined using previous measurements of strong transitions in the ^{150}Eu^{m} and ^{150}Pm decays. The efficiency calibration was made using γ rays at 209.4, 333.9, 406.5, 620.8, 712.3, 831.9, 917.5, 921.7, 1165.8, 1223.1, 1452.6, 1963.5, 2033.4, 2259.8, 2478.6, and 2893.1 keV as well as γ rays at 141.2, 890.6, 1611.8, 1913.2, 2186.2, and 2319.0 keV in ^{90}Nb. The energy calibration used these same transitions along with γ rays at 2614.5 from ^{208}Bi and 2751.8 keV from ^{66}Ga which were also present from contamination.

The gate on the strongest transition at 333.92 keV is shown in Fig. 2 for each decay. The complementary nature of the two decays can be seen, as well as the increased complexity of the ^{150}Pm decay due to its higher Q value.

A. Energy and intensity of γ rays

Intensities determined through both singles and coincidence spectra were generally in agreement. When the coincidence intensity did not agree with the singles intensity, it was found that unresolved multiplets existed. Additionally, some weak peaks were identifiable only in the coincidence spectra. There are a number of weak transitions seen in this study that have not yet been included in the adopted γ's. The energies and intensities of transitions from ^{150}Pm and ^{150}Eu^{m} are given in Appendix A.

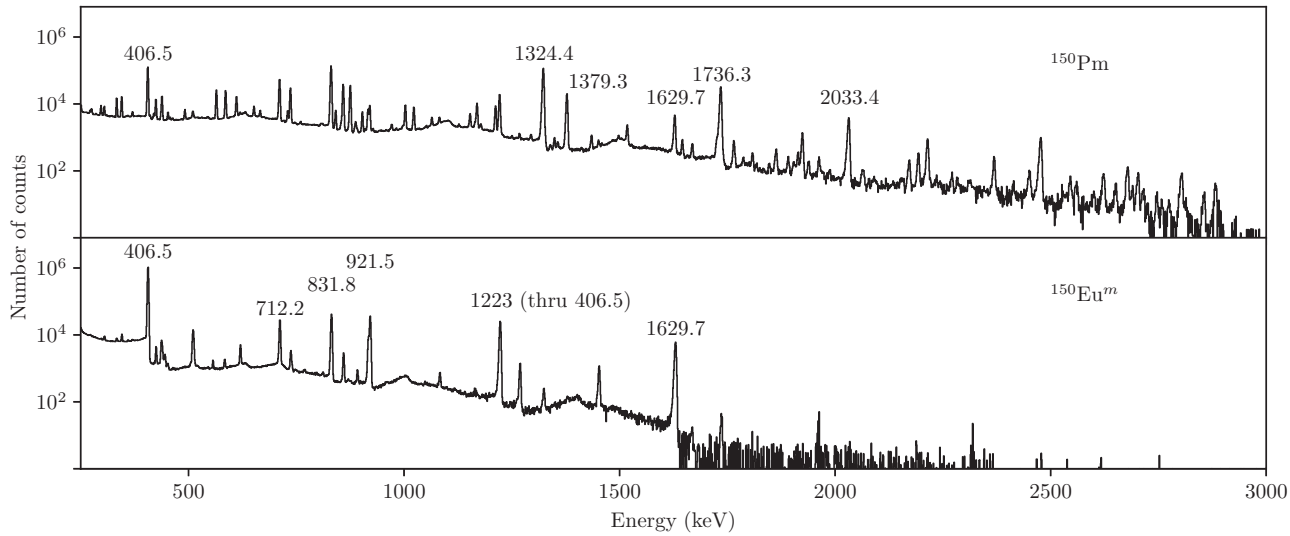

FIG. 2. The 334 keV γ-ray gated γ-coincidence spectrum for ^{150}Pm and ^{150}Eu^m illustrating the increased complexity of ^{150}Pm due to its higher Q value.

B. Levels populated

The energy of each populated level was determined using the uncertainty weighted averages of populating and depopulating γ's in a self-consistent level scheme. When possible, nuclear spins were determined through angular correlation methods, and the parity of the level deduced based on observed level transitions. The energy levels populated in these two decays, either directly or indirectly, are given in Appendix B along with the energy and relative intensity of γ transitions observed, multipolarity, and several relative $B(E2)$ values.

C. Angular correlation measurements

Of particular interest in this study was the determination of the nuclear spins based on the angular distribution of pairs of γ rays. The experimental angular distribution can be written in the form

$$W(\theta) = k[1 + Q_{22}a_2P_2(\cos\theta) + Q_{44}a_4P_4(\cos\theta)], \quad (1)$$

where a_2 and a_4 are the angular correlation coefficients, P_2 and P_4 are Legendre polynomials, Q_{22} and Q_{44} are detector angular-size correction factors, k is a proportionality constant, and $W(\theta)$ is the γ-ray intensity as a function of angle. The

TABLE I. γ-γ angular correlation coefficients from ^{150}Sm 0^+ states populated by the β decay of ^{150}Pm and ^{150}Eu^m.

Initial state	γ-γ	Spin sequence	Decay	Measured		Expected	
				a_2	a_4	a_2	a_4
740	407–334	$0^+(E2)2^+(E2)0^+$	Pm	0.336(21)	1.116(30)	0.357	1.143
			Eu	0.338(16)	1.098(28)	0.357	1.143
1255	922–334	$0^+(E2)2^+(E2)0^+$	Pm	0.307(21)	1.128(34)	0.357	1.143
			Eu	0.343(16)	1.114(28)	0.357	1.143
	209–712	$0^+(E2)2^+(E2+M1)2^+$	Pm	−0.28(4)	0.15(6)	−0.219	0.31
			Eu	−0.153(18)	0.440(24)	−0.219	0.31
	209–1046	$0^+(E2)2^+(E2)0^+$	Eu	0.24(8)	1.14(13)	0.357	1.143
1603	1269–334	$0^+(E2)2^+(E2)0^+$	Pm	0.23(11)	0.92(16)	0.357	1.143
			Eu	0.32(4)	1.18(7)	0.357	1.143
	557–712	$0^+(E2)2^+(E2+M1)2^+$	Eu	−0.25(8)	0.44(10)	−0.219	0.31
	437–832	$0^+(E1)1^-(E1)2^+$	Pm	0.01(8)	−0.08(10)	0.05	0
			Eu	0.06(8)	−0.05(11)	0.05	0
	437–1166	$0^+(E1)1^-(E1)0^+$	Pm	0.58(7)	−0.10(11)	0.5	0
			Eu	0.534(23)	0.07(3)	0.5	0
1787	1453–334	$0^+(E2)2^+(E2)0^+$	Pm	0.02(20)	1.22(23)	0.357	1.143
		$0^+(E2)2^+(E2)0^+$	Eu	0.28(5)	1.03(7)	0.357	1.143
	621–832	$0^+(E1)1^-(E1)2^+$	Pm	0.02(7)	−0.09(10)	0.05	0
			Eu	0.05(4)	−0.07(5)	0.05	0
	621–1166	$0^+(E1)1^-(E1)0^+$	Pm	0.60(7)	−0.06(11)	0.5	0
			Eu	0.46(4)	0.07(6)	0.5	0

correction for angular size of the detectors in this experiment was determined to be $Q_{22} = 0.98(1)$ and $Q_{44} = 0.94(1)$. This was accomplished through a Monte Carlo simulation of the absorption of γ rays over the range of energies in our measurements, using a source-to-detector distance of 22 cm and an average crystal size of 115 cm^3.

The experimental value of $W(\theta)$ was determined by first combining efficiency-corrected counts into five different γ-γ matrices, corresponding to the five different angles that exist within the geometry of the detector array. (Individual detector efficiencies were quite similar, but, in general, this could affect the angular correlation and this correction was still made.) Using proper background subtraction (which was quite important, particularly for weak peaks), the intensity of various peaks in gated spectra were determined for each angle. In this part of the analysis, Compton suppression is quite helpful to reduce the background.

Using five angles with high statistics allows for a relatively precise determination of the angular correlation coefficients using a chi-square minimization technique. Sample fits to determine angular correlation coefficients are shown in Fig. 3.

To help organize the evidence for 0^+ assignments, angular correlation coefficients for γ-γ cascades that originate from a 0^+ state are given in Table I. Angular correlations that involve an $E1$ transition not arising from a 0^+ state are given in Table II. Lastly, angular correlations that involve $E2$+$M1$ or other $E2$ transitions are given in Table III.

It is worth noting the sensitivity of the experiment in determining δ values. The transition between 2_2^+ and 2_1^+ can be explored by utilizing the angular correlation of the 2-2-0 transition corresponding to the 712–334 keV cascade. The values of a_2 and a_4 can then be used together to determine the magnitude and sign of δ. Figure 4 illustrates the technique and the quality of data from the two experiments. The slightly higher statistics from the ^{150}Pm measurement are reflected in the smaller error bars.

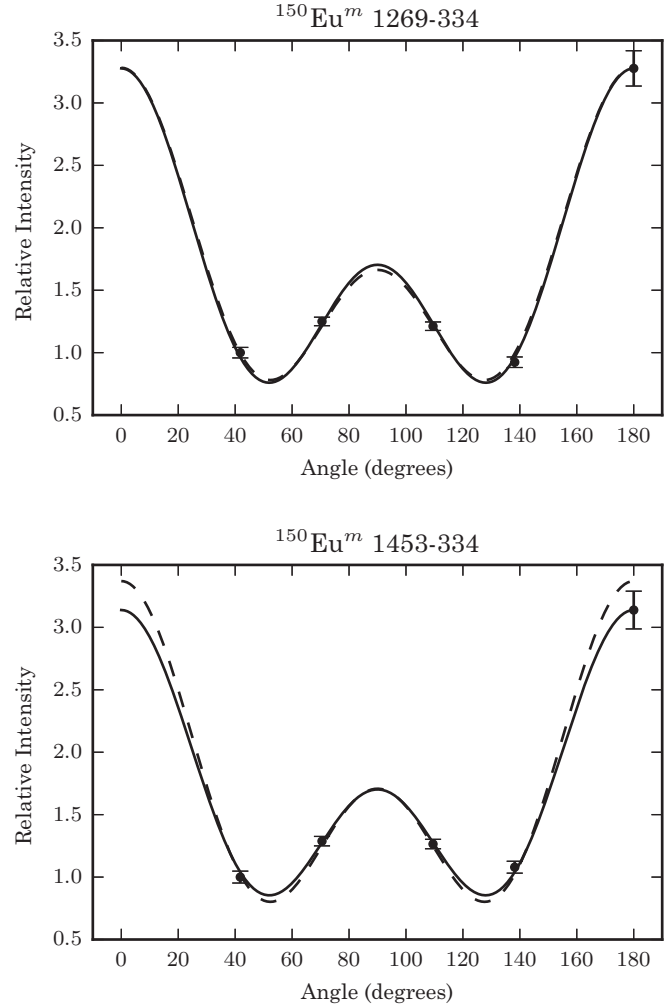

FIG. 3. Example γ-γ angular correlations from ^{150}Eu^m supporting the spin zero assignments for the 1603.24 and 1786.54 keV levels. The dashed line is the theoretical value for a 0-2-0 transition (corrected for the angular size of the detector), and the solid line is the best fit of the $a2$ and $a4$ angular correlation parameters to the data.

D. Comments on levels and γ transitions

Several levels and many transitions were observed in this study that had not been previously identified in these particular β decays. Some of these observations help pin down spin and parity assignments. The observed 272.81(4) keV transition between the 1046.15 and 773.37 levels was questioned by Börner in [13]. As an illustration of the quality of data and method by which we observe and place γ transitions, we see this transition in gates from both feeding (in ^{150}Eu^m in 209 and 918 keV gates, and in ^{150}Pm in 612, 918, 1024, and 1214 keV gates) and clearly in the gate of the depopulating 439 keV transition in both decays as illustrated in Fig. 5.

1. Level and spin assignment of 0^+ for 1603.24 keV level

Evidence for a level around 1603 has at various times appeared in prior experiments, such as that by Humby most recently [12], but only relatively recently was it added to the NDS, with a relatively high uncertainty in energy and only one depopulating γ ray identified.

The 1603.24 keV level was identified in both the ^{150}Eu^m and ^{150}Pm experiments in which the same four depopulating γ rays were observed in each decay. This level was populated to a greater degree in the ^{150}Eu^m decay (as were other 0^+ states). Coincidence gates strongly support all of the γ placements, and two of these γ emissions are clearly seen in the singles spectrum.

The clear 0-2-0 angular correlation in both ^{150}Eu^m and ^{150}Pm strongly indicate a spin 0 assignment (see Table I). Additionally, 0-1-0 angular correlations are seen in both decays, further supporting a spin 0 assignment. Transitions to and from only 2^+ and 1^- levels support a positive parity, and thus a 0^+ assignment.

2. Spin assignment of 0+ for 1786.54 keV level

The 1786.54 keV level had been previously identified as a 0^+ level by Hoshi in 1976 [10], but is currently listed in the Nuclear Data Sheets as $J \leqslant 3$. The 0^+ assignment

TABLE II. γ-γ angular correlation coefficients from ^{150}Sm states involving $E1$ transitions.

Initial state	γ-γ	Spin sequence	Decay	Measured		Expected	
				a_2	a_4	a_2	a_4
1071	737–334	$3^-(E1)2^+(E2)0^+$	Pm	−0.082(11)	0.013(14)	−0.071	0
			Eu	−0.07(6)	−0.05(8)	−0.071	0
	298–439	$3^-(E1)4^+(E2)2^+$	Pm	−0.11(3)	−0.05(4)	−0.14	0
1417	346–737	$2^+(E1)3^-(E1)2^+$	Pm	0.116(22)	0.069(31)	0.12	0
	252–832	$2^+(E1)1^-(E1)2^+$	Pm	−0.03(4)	−0.02(6)	0.005	0
			Eu	−0.01(3)	−0.01(10)	0.005	0
	252–1166	$2^+(E1)1^-(E1)0^+$	Pm	0.04(4)	−0.03(6)	0.05	0
			Eu	0.18(8)	−0.15(10)	0.05	0
1658	1324–334	$2^-(E1)2^+(E2)0^+$	Pm	0.229(8)	0.010(12)	0.25	0
			Eu	0.25(10)	0.04(14)	0.25	0
	612–712	$2^-(E1)2^+(E2+M1)2^+$	Pm	−0.123(18)	−0.05(3)	−0.153	0
	612–1046	$2^-(E1)2^+(E2)0^+$	Pm	0.49(8)	−0.18(11)	0.25	0
1684	1350–334	$3^-(E1)2^+(E2)0^+$	Pm	−0.02(6)	−0.09(9)	−0.071	0
	911–439	$3^-(E1)4^+(E2)2^+$	Pm	−0.26(9)	0.09(12)	−0.14	0
1713	1379–334	$1^-(E1)2^+(E2)0^+$	Pm	−0.233(11)	0.006(14)	−0.25	0
	667–712	$1^-(E1)2^+(E2+M1)2^+$	Pm	0.13(5)	−0.04(7)	0.153	0
1794	628–1166	$2^+(E1)1^-(E1)0^+$	Pm	0.17(14)	−0.15(20)	0.05	0
1964	1630–334	$1^-(E1)2^+(E2)0^+$	Pm	−0.227(20)	−0.030(27)	−0.25	0
			Eu	−0.251(20)	−0.025(26)	−0.25	0
	917–712	$1^-(E1)2^+(E2+M1)2^+$	Pm	0.174(29)	0.03(4)	0.153	0
			Eu	0.101(24)	0.00(3)	0.153	0
2070	1736–334	$2^-(E1)2^+(E2)0^+$	Pm	0.244(11)	−0.016(17)	0.25	0
	653–346	$2^-(E1)2^+(E1)3^-$	Pm	−0.08(3)	−0.05(5)	−0.05	0
	1024–712	$2^-(E1)2^+(E2+M1)2^+$	Pm	−0.168(24)	−0.024(32)	−0.153	0
	1024–1046	$2^-(E1)2^+(E2)0^+$	Pm	0.15(10)	0.04(14)	0.25	0
	876–1194	$2^-(E1)2^+(E2)0^+$	Pm	0.264(13)	−0.035(19)	0.25	0
2226	1180–712	$3^-(E1)2^+(E2+M1)2^+$	Pm	−0.12(10)	−0.08(12)	0.044	0
2260	1926–334	$1^-(E1)2^+(E2)0^+$	Pm	−0.33(4)	−0.00(5)	−0.25	0
	843–346	$1^-(E1)2^+(E1)3^-$	Pm	0.05(3)	−0.04(4)	0.05	0
	1214–712	$1^-(E1)2^+(E2+M1)2^+$	Pm	0.141(23)	0.01(3)	0.153	0
	1214–1046	$1^-(E1)2^+(E2)0^+$	Pm	−0.20(8)	−0.09(11)	−0.25	0
	1066–1194	$1^-(E1)2^+(E2)0^+$	Pm	−0.25(5)	0.12(6)	−0.25	0
2367	2033–334	$2^-(E1)2^+(E2)0^+$	Pm	0.241(23)	0.00(3)	0.25	0
2508	2174–334	$1^-(E1)2^+(E2)0^+$	Pm	−0.37(11)	0.17(13)	−0.25	0
2987	1916–738	$2^+(E1)3^-(E1)2^+$	Pm	0.20(11)	−0.12(15)	0.12	0

is strongly supported from the angular correlations in both ^{150}Eu^m and ^{150}Pm decays. Transitions to and from 2^+ and 1^- levels connecting the 1786.54 level support a positive parity and a 0^+ assignment.

3. Possible levels at 2226.47 keV, 2459.52 keV

In the ^{150}Pm decay, a 2226.47 keV level was observed. Three depopulating γ rays were seen from this level as well as one feeding γ ray. Transitions were seen only to 2^+ and 1^- states. Because of the low intensity of the γ rays, no γ-γ angular correlation information could be obtained, so only a tentative spin-parity assignment of 3^- is proposed.

We observed a level at 2459.52 keV based on only two γ rays, one to the ground state and one to the 1046.15 keV level. Therefore, this level is only tentatively proposed with possible spin assignments of either 1 or 2.

4. Other possible levels between 2500 and 3200 keV

Several higher energy levels are proposed in the consistent decay scheme. Levels at 2607.16(10), 2705.06(7), 2893.06(6), 2895.19(10), 2936.05(8), 2987.15(5), 3025.53(17), and 3071.46(6) keV each have three or more depopulating transitions identified in coincidence gating. Levels at 3093.85(21) and 3191.63(23) keV seem likely with the observation of two depopulating γ emissions.

IV. DISCUSSION AND SUMMARY

Using the 8π spectrometer we have measured the γ emissions from the β decays of ^{150}Eu^m and ^{150}Pm. In the ^{150}Eu^m decay we have placed 57 γ transitions (only 18 of which are listed in the Nuclear Data Sheets), and in the ^{150}Pm decay 209 γ transitions (57 of which are listed in the Nuclear Data Sheets), all in a self-consistent level scheme. All of these transitions are placed through coincidence gating. Numerous

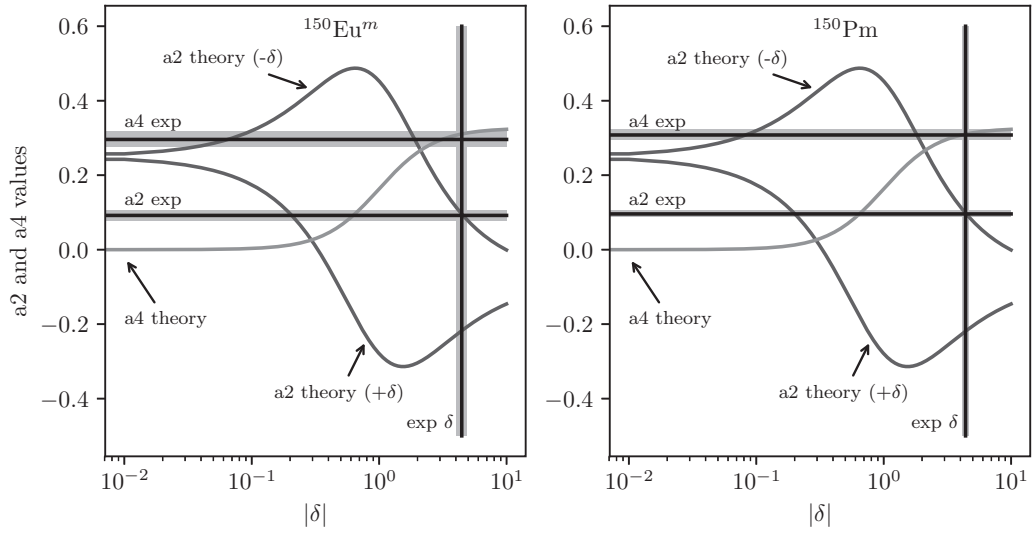

FIG. 4. Determining the experimental value for δ from the experimental values of a_2 and a_4 in the 712–334 keV (2-2-0) γ cascade. The value of δ is determined by locating where the a_2 and a_4 experimental values cross the theory curves at a consistent value of δ. Both experiments yielded consistent results arriving at $\delta = -4.45(43)$ and $\delta = -4.40(27)$ for ^{150}Eu^m and ^{150}Pm respectively. Uncertainties in the experimental values are indicated with the lighter gray bar.

angular correlation coefficients were measured, confirming, correcting, or narrowing down many previous spin assignments. We found that a high-statistics measurement with a Compton-suppressed detector array, in a geometry with many repeated angles of detector pairs, allowed for angular correlation measurements of even fairly weak transitions. The

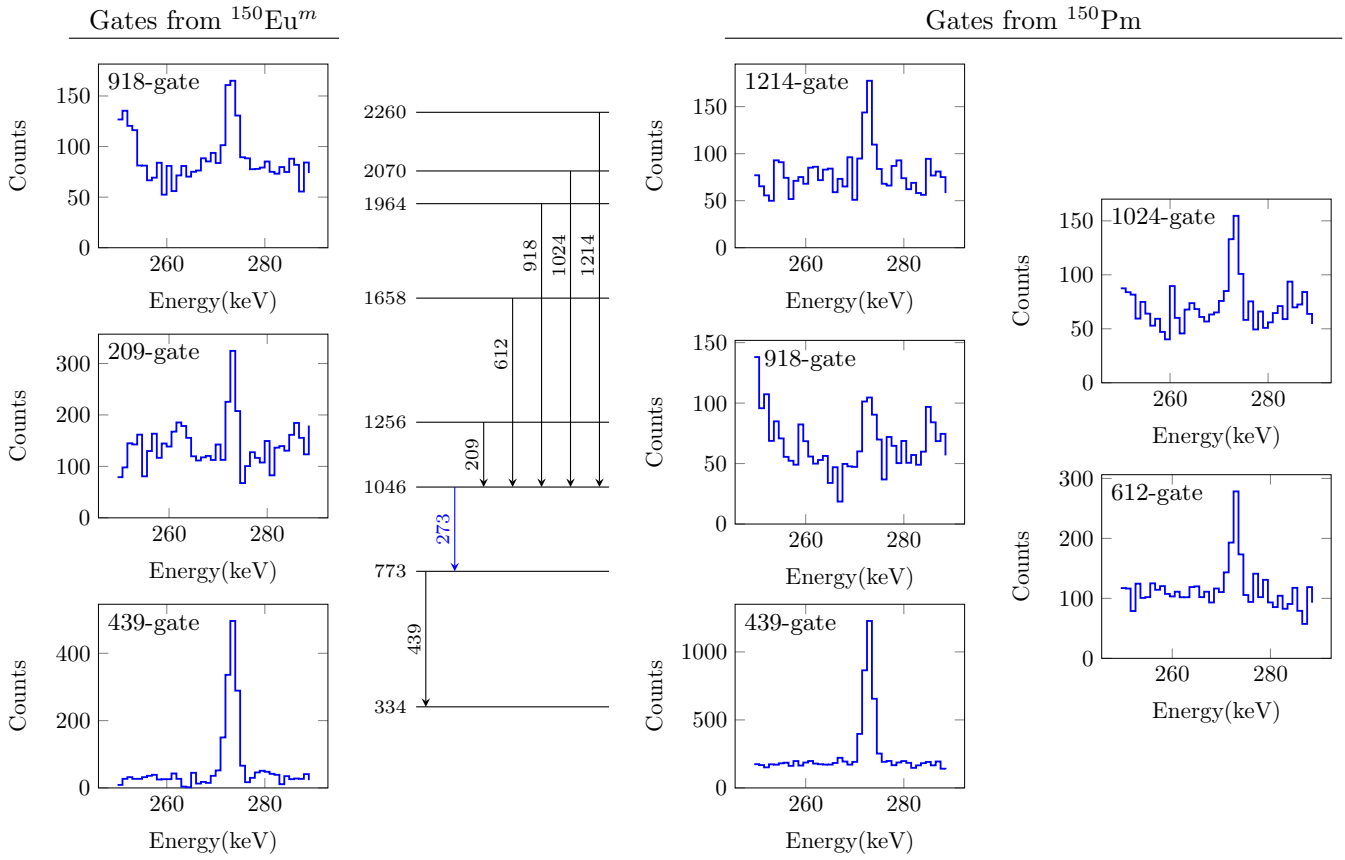

FIG. 5. Partial decay scheme of ^{150}Sm and the gates supporting the 272.81(4) keV transition between the 1046.15 and 773.37 keV levels.

TABLE III. γ-γ angular correlations involving $E2$ or $E2/M1$ transitions.

Initial state	γ-γ	Spin sequence	Decay	Measured		Expected a_2, a_4 or $\delta(E2/M1)$
				a_2	a_4	
773	439–334	$4^+(E2)2^+(E2)0^+$	Pm	0.135(15)	0.036(22)	$a_2 = 0.102$, $a_4 = 0.009$
1046	712–334	$2^+(E2+M1)2^+(E2)0^+$	Pm	0.096(9)	0.308(13)	$\delta(712) = -4.39(27)$
			Eu	0.092(14)	0.296(21)	$\delta(712) = -4.45(43)$
	273–439	$2^+(E2)4^+(E2)2^+$	Pm	0.26(7)	0.20(10)	$a_2 = 0.102$, $a_4 = 0.009$
1194	860–334	$2^+(E2+M1)2^+(E2)0^+$	Pm	−0.294(9)	0.270(12)	$\delta(860) = 2.17(19)$
			Eu	−0.220(31)	0.31(4)	$\delta(860) = 4.3(16)$
	420–439	$2^+(E2)4^+(E2)2^+$	Pm	0.26(5)	0.10(7)	$a_2 = 0.102$, $a_4 = 0.009$
1417	1083–334	$2^+(E2+M1)2^+(E2)0^+$	Pm	−0.23(4)	0.43(6)	$\lvert\delta(1083)\rvert > = 4.6$
			Eu	0.02(7)	0.24(10)	$\lvert\delta(1083)\rvert > = 7.5$
	371–712	$2^+(E2+M1)2^+(E2+M1)2^+$	Pm	−0.18(6)	0.19(8)	$\delta(371) = -2.1(6)$
1505	1171–334	$3^+(E2+M1)2^+(E2)0^+$	Pm	−0.123(16)	−0.074(21)	$\delta(1171) = 10.0(16)$
	731–439	$3^+(E2+M1)4^+(E2)2^+$	Pm	−0.114(31)	−0.17(4)	$\delta(731) = 6.5(14)$
1658	587–738	$2^-(E2+M1)3^-(E1)2^+$	Pm	0.186(15)	0.009(22)	$\delta(587) = 0.052(5)$
	493–1166	$2^-(E2+M1)1^-(E1)0^+$	Pm	0.51(4)	0.05(6)	$\delta(493) = -1.3(10)$
2004	1670–334	$2^+(E2+M1)2^+(E2)0^+$	Pm	0.27(7)	0.07(10)	$\delta(1670) = -0.032(12)$
2070	999–737	$2^-(E2+M1)3^-(E1)2^+$	Pm	0.40(10)	0.11(15)	$\delta(999) = 0.8(5)$
	904–832	$2^-(E2+M1)1^-(E1)2^+$	Pm	0.05(3)	−0.02(5)	
	904–1166	$2^-(E2+M1)1^-(E1)0^+$	Pm	0.21(3)	−0.05(5)	$\delta(904) = -0.23(2)$
2367	1296–738	$2^-(E2+M1)3^-(E1)2^+$	Pm	0.34(10)	0.03(14)	$\delta(1296) = -1.3(3)$
2602	1437–1166	$2^-(E2+M1)1^-(E1)0^+$	Pm	0.51(7)	0.19(10)	$\delta(1437) = -1.7(10)$
2813	1767–712	$2^+(E2+M1)2^+(E2+M1)2^+$	Pm	−0.11(7)	0.00(10)	
2893	1728–1166	$2^-(E2+M1)1^-(E1)0^+$	Pm	0.30(8)	0.18(11)	$\delta(1728) = -0.42(18)$

spin assignments of 0^+ to the 1603.24 and 1786.54 keV levels are of importance because 0^+ levels are particularly restrictive to theory, which is important in the poorly understood $N = 88$ region.

The structure of ^{150}Sm has been discussed using a wide range of models. Most recently, Börner *et al.* [13] addressed the evidence for a phase transition between spherical and quadrupole axial symmetric shapes, placing this nucleus just prior to the critical point on the spherical side of the transition, and Gupta *et al.* [19] explored fits of various collective models to selected data. However, there is long-standing evidence for multiple shape coexistence in this nucleus (see Figs. 3.35 in [20] and Fig. 18 in [21]). In particular, the 0^+, 2^+, and 4^+ states at 1256, 1417, and 1819 keV are consistent, based on γ-ray branching ratios, with a strongly deformed band; this band is strongly populated in two-neutron pickup reactions from the more-deformed nucleus ^{152}Sm (see Fig. 3.34 in [20]). However, no lifetime data are available. Further, the quadrupole moment of the first 2^+ state is large [22], which challenges the notion that this nucleus is close to being spherical. From the multiple spectroscopic studies of the neighboring nucleus, ^{152}Sm (see [6] and references therein), that support nearly degenerate shape coexistence with strong mixing [23], it is evidently desirable to also study ^{150}Sm by multiple spectroscopic techniques.

The new 0^+ state at 1603 keV and the confirmed 0^+ state at 1786 keV are critical challenges for collective models. Formerly, it would have been natural to consider them in a multiphonon picture, either associated with spherical quadrupole vibrations or deformed β and γ vibrations. However, serious doubt has been cast on spherical quadrupole vibrations at the multiphonon level [24], and β vibrations likewise are in serious doubt [25–27]. The most natural interpretation would involve nucleon-pair degrees of freedom, such as manifest in shape coexistence [28] and in "pairing vibrations" [29–31].

ACKNOWLEDGMENTS

The authors wish to thank the staff at the 88-inch cyclotron for their assistance. This material is based on work supported by DOE Grants/Contracts No. DE-FG03-98ER41060 (OSU), No. DE-FG0296ER40958 (Ga Tech), and No. DE-AC03-76SF00098 (LBNL).

APPENDIX A: γ-RAY INTENSITIES

Due to the complementary nature of the decays, transitions observed from ^{150}Pm and ^{150}Eu^m are shown together in Table IV. For both decays, the intensity was normalized to 100.0 units for the strongest transition of 333.92 keV. (Because each is normalized to the strongest transition only, the intensities differ between the two decays, but the presence of the transitions can be seen.) Data from the Nuclear Data Sheets are shown for comparison in this table. There are a number of weak transitions seen in this study that have not yet been included in the adopted γ's.

APPENDIX B: OBSERVED LEVELS AND γ TRANSITIONS

The energy levels populated in these two decays, either directly or indirectly, are given in Table V. Additionally this table includes the energy and relative intensity of γ tran-

TABLE IV. Gamma ray intensities from the β decay of $^{150}Eu^{m}$ and ^{150}Pm. Relative photon intensities are normalized to the strongest γ transition at 100.0 units.

^{150}Pm				$^{150}Eu^{m}$				Levels (keV)	
Present work		Nuclear Data Sheets		Present work		Nuclear Data Sheets		Initial	Final
E (keV)	I	E (keV)	I	E (keV)	I	E (keV)	I		
90.05(15)	0.08(4)[b]			89.74(5)	0.11(6)[b]			1255.48	1165.77
120.2(5)	0.0082(23)[b]							1165.77	1046.15
148.0(5)	0.008(4)[b]							1193.85	1046.15
153.75(20)	0.0113(25)[b]							1658.38	1504.57
162.21(20)	0.0068(22)[b]							1417.37	1255.48
209.42(7)	0.104(6)	209.45(12)	0.09(2)	209.24(4)	0.637(23)	209.4(1)	0.55(8)	1255.48	1046.15
223.76(21)	0.0090(23)	225.0(8)	≈0.01[a]	223.66(10)	0.0055(24)[b]			1417.37	1193.85
237.1(8)	0.050(4)	237.4(6)	0.06(1)[a]					2070.25	1833.52
241.08(18)	0.0067(13)	241.5(4)	≈0.02					1658.38	1417.37
242.2(3)	0.0054(6)							1926.54	1684.29
				250.45(20)	0.0036(7)[b]			1963.59	1713.25
251.65(4)	0.279(17)	251.60(10)	0.26(4)	251.57(7)	0.085(11)[b]			1417.37	1165.77
272.82(4)	0.058(3)	272.8(10)	0.09(3)	272.66(13)	0.0305(25)			1046.15	773.37
276.35(4)	0.150(8)	276.5(5)	0.14(5)					2070.25	1794.03
279.06(22)	0.0051(7)[b]			279.17(12)	0.0036(9)[b]			1963.59	1684.29
298.04(4)	0.203(11)	297.9(2)	0.17(3)	297.99(8)	0.020(6)			1071.42	773.37
				305.16(10)	0.0088(18)[b]			1963.59	1658.38
305.68(4)	0.192(10)	305.7(2)	0.16(3)	305.61(7)	0.114(10)	305.4(4)	≈0.08	1046.15	740.45
310.71(6)	0.043(7)[b]							1504.57	1193.85
333.94(4)	100(5)	333.92(3)	100	333.88(3)	100(3)	333.9(1)	100(8)	333.93	0
345.92(4)	0.66(3)	345.93(8)	0.64(7)	345.91(4)	0.214(11)			1417.37	1071.42
356.93(8)	0.0214(23)							2070.25	1713.25
360.30(5)	0.044(3)			360.40(14)	0.049(5)			1963.59	1603.24
362.91(15)	0.0036(26)							2367.4	2004.4
				369.03(12)	0.069(8)			1786.54	1417.37
371.16(6)	0.116(7)			371.19(6)	0.041(3)			1417.37	1046.15
375.91(19)	0.0101(26)							2602.29	2226.47
385.87(15)	0.0055(8)							2070.25	1684.29
406.50(4)	8.9(4)	406.51(3)	8.2(5)	406.49(4)	75(2)	406.5(1)	71(6)	740.45	333.93
409.8(3)	0.013(4)[b]			409.37(11)	0.0181(22)[b]			1603.24	1193.85
411.89(12)	0.086(6)							2070.25	1658.38
420.44(4)	0.120(7)	420.1(5)	0.16(3)	420.23(20)	0.0063(8)[b]			1193.85	773.37
425.32(4)	0.76(4)	425.33(7)	0.71(8)	425.28(5)	0.249(8)	425.3(3)	0.20(4)	1165.77	740.45
426.27(16)	0.0143(14)[b]							2259.79	1833.52
437.47(5)	0.205(13)			437.39(4)	0.71(5)			1603.24	1165.77
439.44(4)	0.99(5)	439.38(7)	1.13(8)	439.36(5)	0.045(16)			773.37	333.93
453.38(4)	0.201(11)	453.48(16)	0.21(4)	453.47(10)	0.0187(19)			1193.85	740.45
458.39(6)	0.059(4)	458.4(2)	0.05(1)					1504.57	1046.15
464.49(6)	0.069(8)	465.1(6)	0.07(1)					1658.38	1193.85
492.65(4)	0.57(3)	492.56(8)	0.50(6)					1658.38	1165.77
532.07(20)	0.022(4)	532.3(8)	0.04(2)					2602.29	2070.25
545.15(12)	0.023(5)							2367.4	1822.26
				546.19(14)	0.0280(28)			1963.59	1417.37
546.50(23)	0.0037(8)[b]							2259.79	1713.25
547.56(13)	0.046(4)	547.4(8)	0.06(2)					1713.25	1165.77
557.28(18)	0.0159(23)			557.10(6)	0.083(4)			1603.24	1046.15
565.72(4)	2.03(10)	565.70(3)	1.93(14)					2070.25	1504.57
587.02(4)	1.96(10)	587.02(8)	1.97(14)	586.5(3)	0.0035(7)[b]			1658.38	1071.42
				592.60(21)	0.0106(29)			1786.54	1193.85
600.32(10)	0.023(6)			600.1(4)	0.0030(9)[b]			1794.03	1193.85
612.18(4)	1.39(7)	612.25(8)	1.37(10)					1658.38	1046.15
620.68(5)	0.221(15)	620.8(4)	0.18(3)	620.83(5)	0.840(26)	620.3(2)	0.80(12)	1786.54	1165.77

TABLE IV. *(Continued.)*

^{150}Pm				^{150}Eu^{m}				Levels (keV)	
Present work		Nuclear Data Sheets		Present work		Nuclear Data Sheets		Initial	Final
E (keV)	I	E (keV)	I	E (keV)	I	E (keV)	I		
628.31(9)	0.060(6)							1794.03	1165.77
633.03(15)	0.135(8)	633.5(6)	0.10(2)					2893.06	2259.79
652.90(5)	0.512(27)	652.84(9)	0.49(6)					2070.25	1417.37
656.70(10)	0.0149(27)							2259.79	1603.24
667.13(5)	0.246(14)	667.3(3)	0.23(4)					1713.25	1046.15
667.6(9)	0.020(4)[b]							1833.52	1165.77
675.95(17)	0.032(5)							2936.05	2259.79
683.06(20)	0.0081(16)[b]							2367.4	1684.29
708.03(20)	0.023(3)[b]			707.90(9)	0.025(5)[b]			1963.59	1255.48
709.13(20)	0.033(8)							2367.4	1658.38
712.24(4)	6.05(30)	712.22(4)	6.4(4)	712.31(5)	3.44(10)	712.2(1)	3.3(3)	1046.15	333.93
722.46(9)	0.030(3)			723.4(3)	0.0025(7)[b]			1794.03	1071.42
731.25(4)	0.418(22)	731.06(16)	0.41(7)					1504.57	773.37
737.47(4)	3.07(15)	737.50(8)	3.31(23)	737.59(6)	0.308(12)			1071.42	333.93
				740.44(6)	0.021(3)[b]			1786.54	1046.15
740.5(3)	0.061(10)							2705.06	1963.59
747.86(8)	0.032(5)[b]			748.2(4)	0.0080(20)[b]			1794.03	1046.15
760.79(9)	0.076(9)[b]							1926.54	1165.77
762.07(10)	0.0241(23)[b]							1833.52	1071.42
769.81(17)	0.025(6)[b]			769.73(11)	0.046(5)			1963.59	1193.85
				797.88(21)	0.019(4)			1963.59	1165.77
808.6(3)	0.032(6)[b]							2812.96	2004.4
811.66(9)	0.043(9)[b]							3071.46	2259.79
831.81(4)	17.0(9)	831.85(4)	17.5(7)	831.93(6)	5.64(17)	831.8(1)	5.0(4)	1165.77	333.93
837.58(20)	0.0110(17)[b]							2550.56	1713.25
842.50(4)	0.72(4)	842.55(12)	0.60(7)					2259.79	1417.37
855.08(12)	0.106(7)							1926.54	1071.42
859.88(4)	4.85(24)	859.95(4)	5.0(3)	860.01(7)	0.352(11)	860.1(5)	0.23(6)	1193.85	333.93
862.11(9)	0.055(11)[b]							2812.96	1950.83
871.06(20)	0.015(3)[b]							2529.39	1658.38
876.39(4)	10.6(5)	876.41(4)	10.7(5)	876.58(16)	0.016(4)			2070.25	1193.85
886.62(10)	0.111(10)							2812.96	1926.54
889.03(6)	0.194(12)	889.2(5)	0.21(4)					2602.29	1713.25
892.21(7)	0.047(3)			892.12(9)	0.084(4)			1963.59	1071.42
904.49(4)	1.32(7)	904.46(8)	1.34(9)					2070.25	1165.77
910.88(7)	0.054(4)	911.0(6)	0.10(2)					1684.29	773.37
917.46(4)	0.82(4)	917.44(16)	0.70(10)	917.54(7)	1.25(4)	917.7(6)	1.1(2)	1963.59	1046.15
921.49(4)	1.12(5)	921.61(16)	1.25(10)	921.67(7)	5.85(18)	921.7(3)	5.3(4)	1255.48	333.93
926.06(10)	0.0165(25)							2529.39	1603.24
929.30(9)	0.065(6)							2893.06	1963.59
968.83(13)	0.034(6)							2895.19	1926.54
972.77(8)	0.153(10)	972.2(8)	0.14(2)					1713.25	740.45
982.67(24)	0.044(5)							2987.15	2004.4
990.4(3)	0.0022(11)[b]							2812.96	1822.26
998.76(9)	0.073(6)	999.0(10)	0.09(3)					2070.25	1071.42
1004.23(4)	1.34(7)	1004.44(12)	1.18(8)					2259.79	1255.48
1024.00(4)	1.11(6)	1024.13(6)	1.08(8)	1024.5(3)	0.0027(5)[b]			2070.25	1046.15
1032.69(10)	0.027(4)[b]							2226.47	1193.85
1036.23(9)	0.028(5)							2987.15	1950.83
1046.10(6)	0.535(28)	1046.12(8)	0.52(6)	1046.20(8)	0.272(11)	1046.2(3)	0.21(5)	1046.15	0
1048.86(17)	0.0182(19)[b]							1822.26	773.37
1053.53(9)	0.046(4)			1053.3(4)	0.008(3)[b]			1794.03	740.45
1059.98(18)	0.0085(13)[b]							1833.52	773.37

TABLE IV. *(Continued.)*

^{150}Pm				^{150}Eu^{m}				Levels (keV)	
Present work		Nuclear Data Sheets		Present work		Nuclear Data Sheets		Initial	Final
E (keV)	I	E (keV)	I	E (keV)	I	E (keV)	I		
1061.1(4)	0.012(5)[b]							2226.47	1165.77
1065.90(4)	0.68(4)	1066.00(16)	0.66(7)					2259.79	1193.85
1083.39(6)	0.234(15)	1083.33(8)	0.26(4)	1083.58(10)	0.086(4)			1417.37	333.93
1090.68(20)	0.013(3)[b]							2507.79	1417.37
1093.94(15)	0.049(8)	1093.5(8)	0.11(2)					2259.79	1165.77
1101.77(16)	0.0117(22)[b]							2705.06	1603.24
1128.60(11)	0.053(5)	1128.6(8)	0.10(2)					2812.96	1684.29
1133.02(23)	0.0111(20)							2550.56	1417.37
1153.5(4)	0.0199(20)							1926.54	773.37
1154.57(5)	0.68(4)	1154.64(16)	1.00(7)					2812.96	1658.38
1165.77(5)	23(1)	1165.77(6)	23.3(9)	1165.80(9)	6.97(21)	1165.7(2)	6.5(6)	1165.77	0
1170.60(5)	1.49(8)	1170.9(3)	1.56(18)					1504.57	333.93
1173.67(10)	0.101(10)[b]							2367.4	1193.85
1177.44(8)	0.054(4)[b]							1950.83	773.37
1179.92(11)	0.044(4)[b]	1179.6(6)	0.15(3)					2893.06	1713.25
1180.28(7)	0.107(7)[b]							2226.47	1046.15
1188.54(17)	0.0161(23)[b]							2259.79	1071.42
1193.86(5)	6.9(3)	1193.87(6)	7.1(4)	1193.91(9)	0.457(14)	1193.7(2)	0.46(10)	1193.85	0
1201.77(21)	0.036(7)	1201.8(5)	0.11(2)					2367.4	1165.77
1210.3(8)	0.0106(19)[b]							2895.19	1684.29
1213.65(5)	1.49(8)	1213.72(8)	1.52(11)					2259.79	1046.15
1223.14(5)	3.60(18)	1223.28(6)	4.16(29)	1223.13(9)	5.47(16)	1223.0(2)	5.0(4)	1963.59	740.45
1251.84(16)	0.024(3)							2936.05	1684.29
1263.95(16)	0.0154(23)							2004.4	740.45
1269.37(13)	0.088(6)			1269.30(10)	0.312(11)			1603.24	333.93
1295.02(22)	0.0082(14)							2550.56	1255.48
1296.05(9)	0.077(6)[b]							2367.4	1071.42
1308.4(4)	0.015(3)[b]							2812.96	1504.57
1324.45(5)	23(1)	1324.51(6)	25.7(10)	1324.57(26)	0.037(5)			1658.38	333.93
1328.83(10)	0.154(12)							2987.15	1658.38
1350.36(8)	0.101(7)	1350.7(5)	0.13(2)	1349.99(22)	0.0010(3)[b]			1684.29	333.93
1358.20(11)	0.055(5)							3071.46	1713.25
1363.9(4)	0.016(4)[b]	1364.1(8)	0.03(1)[a]					2529.39	1165.77
1379.31(5)	4.09(21)	1379.32(6)	4.63(32)	1379.3(3)	0.0135(29)			1713.25	333.93
1413.2(3)	0.0102(24)[b]							2607.16	1193.85
1413.37(16)	0.0144(27)[b]							2459.52	1046.15
1417.1(4)	0.008(6)							1417.37	0
1436.52(7)	0.355(24)	1436.6(4)	0.39(7)[a]					2602.29	1165.77
1448.7(3)	0.0062(14)[b]							2705.06	1255.48
1452.80(13)	0.066(6)	1452.9(10)	0.19(5)	1452.59(11)	0.323(11)	1452.3(2)	0.37(13)	1786.54	333.93
1455.4(3)	0.0033(15)[b]							3139.5	1684.29
1460.3(4)	0.022(4)							1794.03	333.93
1461.7(3)	0.008(4)[b]							2507.79	1046.15
1499.58(10)	0.057(8)	1499.6(6)	0.11(2)					1833.52	333.93
1504.6(3)	0.0089(18)[b]							2550.56	1046.15
1519.34(6)	0.426(23)	1519.53(12)	0.39(7)					2259.79	740.45
1561.27(18)	0.0132(22)[b]							2607.16	1046.15
1570.41(25)	0.0064(16)[b]							2987.15	1417.37
1616.3(5)	0.0040(8)[b]							1950.83	333.93
1629.68(5)	1.04(5)	1629.79(4)	1.17(8)	1629.65(13)	1.72(5)	1629.4(3)	1.45(19)	1963.59	333.93
1634.85(21)	0.018(4)[b]							3139.5	1504.57
1647.17(7)	0.329(23)	1647.20(25)	0.37(6)					2812.96	1165.77
1670.46(8)	0.111(7)	1670.7(5)	0.13(2)[a]					2004.4	333.93

TABLE IV. *(Continued.)*

^{150}Pm				^{150}Eu^{m}				Levels (keV)	
Present work		Nuclear Data Sheets		Present work		Nuclear Data Sheets		Initial	Final
E (keV)	I	E (keV)	I	E (keV)	I	E (keV)	I		
1713.19(11)	0.523(27)	1713.31(12)	0.52(6)					1713.25	0
1727.51(6)	0.334(24)	1726.9(6)	0.28(5)					2893.06	1165.77
1736.31(5)	8.7(4)	1736.40(8)	10.2(5)	1736.31(18)	0.0101(14)[b]			2070.25	333.93
1741.53(16)	0.034(3)[b]							2812.96	1071.42
1766.78(9)	0.197(13)	1766.7(3)	0.28(5)					2812.96	1046.15
1770.20(21)	0.038(5)							2936.05	1165.77
1788.87(14)	0.0281(24)	1789.8(8)	0.02(1)					2529.39	740.45
1793.96(21)	0.019(3)							1794.03	0
1810.05(10)	0.065(5)	1810.5(6)	0.06(2)					2550.56	740.45
1833.64(16)	0.0264(24)	1833.3(10)	0.04(3)[a]					1833.52	0
1849.09(21)	0.0149(21)	1848.0(10)	≈0.005[a]					2895.19	1046.15
1864.73(11)	0.049(4)							2936.05	1071.42
1866.63(22)	0.0107(13)[b]							2607.16	740.45
1905.70(9)	0.075(8)	1906.3(6)	0.11(2)[a]					3071.46	1165.77
1915.71(9)	0.077(6)	1915.9(6)	0.11(2)[a]					2987.15	1071.42
1925.88(6)	0.359(20)	1926.04(8)	0.50(10)					2259.79	333.93
1940.94(9)	0.0193(23)[b]	1940.6(3)	0.10(2)[a]					2987.15	1046.15
1963.60(5)	2.25(11)	1963.71(8)	2.16(15)	1963.55(16)	2.99(9)	1963.0(3)	2.9(3)	1963.59	0
1964.63(11)	0.035(3)[b]							2705.06	740.45
1973.57(21)	0.013(12)							3139.5	1165.77
2004.2(4)	0.0043(14)	2003.4(10)	0.04(2)[a]					2004.4	0
2033.37(5)	1.19(6)	2033.46(8)	1.42(10)					2367.4	333.93
2067.6(3)	0.0089(18)[b]							3139.5	1071.42
2120.3(3)	0.0041(15)							2893.06	773.37
2154.3(3)	0.0045(10)							2895.19	740.45
2173.81(7)	0.057(4)	2173.7(8)	0.08(3)					2507.79	333.93
2195.41(6)	0.102(6)	2195.6(6)	0.13(3)					2529.39	333.93
2216.61(12)	0.286(16)	2216.5(3)	0.35(6)					2550.56	333.93
2259.78(14)	0.108(6)	2259.8(8)	0.10(3)					2259.79	0
2273.08(15)	0.0154(19)							2607.16	333.93
2285.03(23)	0.0140(19)							3025.53	740.45
2310.2(4)	0.0040(9)[b]							3050.56	740.45
2371.21(13)	0.082(5)							2705.06	333.93
2459.5(4)	0.0096(14)							2459.52	0
2479.03(13)	0.371(20)	2478.6(2)	0.55(6)					2812.96	333.93
2507.91(14)	0.085(5)	2507.3(6)	0.08(3)					2507.79	0
2529.49(13)	0.522(27)	2529.2(3)	0.49(6)					2529.39	0
2550.51(15)	0.204(11)	2550.5(5)	0.18(4)					2550.56	0
2560.7(3)	0.0125(16)[b]							2895.19	333.93
2601.9(5)	0.0063(11)							2936.05	333.93
2607.2(5)	0.0132(20)							2607.16	0
2653.1(3)	0.0135(16)							2987.15	333.93
2691.6(3)	0.0094(14)	2691.0(8)	0.010(5)					3025.53	333.93
2704.84(19)	0.0338(28)	2704.6(7)	0.06(3)					3038.81	333.93
2716.56(26)	0.0112(13)	2716.1(8)	0.010(5)					3050.56	333.93
2748.5(3)	0.0069(12)							3082.21	333.93
2760.06(23)	0.0045(9)							3093.85	333.93
2805.76(18)	0.038(3)	2804.2(5)	0.07(3)					3139.5	333.93
2857.74(24)	0.0075(11)							3191.63	333.93
2895.3(3)	0.303(16)	2893.1(5)	0.31(5)[a]					2895.19	0
3025.4(4)	0.0390(25)	3022.7(20)	0.04(1)					3025.53	0
3038.8(4)	0.0197(14)	3037.8(10)	0.02(1)					3038.81	0
3050.5(4)	0.0157(12)	3049.7(10)	0.02(1)					3050.56	0

TABLE IV. *(Continued.)*

^{150}Pm				^{150}Eu^{m}				Levels (keV)	
Present work		Nuclear Data Sheets		Present work		Nuclear Data Sheets		Initial	Final
E (keV)	I	E (keV)	I	E (keV)	I	E (keV)	I		
3081.6(5)	0.0247(17)	3079.8(10)	0.02(1)					3082.21	0
3093.0(5)	0.0106(9)	3090.5(10)	≈0.01					3093.85	0
3140.1(6)	0.0047(7)	3137.3(10)	≈0.003					3139.5	0
3191.1(6)	0.0030(4)							3191.63	0

[a]NDS gives a placement different from that of the present work.
[b]Intensity was determined only through coincidence gating (such as a very weak peak or unresolved doublet.)

sitions observed, along with their multipolarity, and several relative $B(E2)$ values. When particular γ-ray transitions were observed in both decays, their energy and intensity values were combined using their uncertainty weighted averages. The uncertainty quoted in the weighted average is the higher of the internal and external uncertainty. In the few cases of

TABLE V. Observed levels and relative γ intensities of ^{150}Sm derived from the decays of ^{150}Pm and ^{150}Eu^{m}. Energies, intensities, and their uncertainties are determined using their weighted average.

NDS		Present work							
E (keV)	J^{π}	E_{level}	J^{π}	E_{γ} (keV)	I_{γ}	γ mult.	$B(E2)_{\text{rel}}$	E_{final}	J^{π}_{f}
333.955(10)	2^{+}	333.926(18)	2^{+}	333.906(24)	100(3)	$E2$		0	0^{+}
740.464(19)	0^{+}	740.447(22)	0^{+}	406.494(26)	100(3)	$E2$		333.926(18)	2^{+}
773.374(12)	4^{+}	773.37(4)	4^{+}	439.411(29)	100(5)	$E2$		333.926(18)	2^{+}
1046.148(13)	2^{+}	1046.150(19)	2^{+}	272.80(4)	0.94(4)	$E2$	52(3)	773.37(4)	4^{+}
				305.67(3)	3.20(15)	$E2$	100(5)	740.447(22)	0^{+}
				712.260(30)	100(3)	95% $E2$	43(1)	333.926(18)	2^{+}
				1046.13(5)	8.2(4)	$E2$	0.55(1)	0	0^{+}
1071.406(12)	3^{-}	1071.421(26)	3^{-}	298.03(3)	6.6(3)	$E1$		773.37(4)	4^{+}
				737.50(3)	100(3)	$E1$		333.926(18)	2^{+}
1165.791(17)	1^{-}	1165.765(22)	1^{-}	120.2(5)	0.036(10)	$E1$		1046.150(19)	2^{+}
				425.306(28)	3.50(10)	$E1$		740.447(22)	0^{+}
				831.84(3)	79.2(28)	$E1$		333.926(18)	2^{+}
				1165.78(5)	100(3)	$E1$		0	0^{+}
1193.843(12)	2^{+}	1193.847(25)	2^{+}	148.0(5)	0.12(5)	$M1+E2$	$<10^{3}$	1046.150(19)	2^{+}
				420.43(4)	1.65(17)	$E2$	79(4)	773.37(4)	4^{+}
				453.39(3)	3.5(6)[a]	$E2$	100(5)	740.447(22)	0^{+}
				859.91(3)	75(3)	83% $E2$	83(3)	333.926(18)	2^{+}
				1193.87(5)	100(3)	$E2$	25.8(7)	0	0^{+}
1255.512(20)	0^{+}	1255.480(25)	0^{+}	89.77(5)	2.3(14)	$E1$		1165.765(22)	1^{-}
				209.28(3)	10.0(8)[a]	$E2$	100(3)	1046.150(19)	2^{+}
				921.53(3)	100(3)	$E2$	0.58(2)	333.926(18)	2^{+}
1417.346(13)	2^{+}	1417.366(21)	2^{+}	162.21(20)	1.0(3)	$E2$	100(32)	1255.480(25)	0^{+}
				223.68(9)	1.5(3)	$M1+E2$	<28(6)	1193.847(25)	2^{+}
				251.63(4)	41.6(23)	$E1$		1165.765(22)	1^{-}
				345.914(28)	100(4)	$E1$		1071.421(26)	3^{-}
				371.17(4)	18.1(9)	82% $E2$	23(3)	1046.150(19)	2^{+}
				1083.44(5)	38.3(25)	>95% $E2$	0.27(2)	333.926(18)	2^{+}
				1417.1(4)	1.2(9)	$E2$	0.002(1)	0	0^{+}
1504.572(13)	3^{+}	1504.574(29)	3^{+}	310.71(6)	2.9(5)	91% $E2$	100(17)	1193.847(25)	2^{+}
				458.39(6)	3.94(27)	100% $E2$	19.7(14)	1046.150(19)	2^{+}
				731.25(4)	27.9(15)	98% $E2$	14.5(7)	773.37(4)	4^{+}
				1170.60(5)	100(5)	99% $E2$	4.99(28)	333.926(18)	2^{+}
1603.(4)		1603.24(4)	0^{+}	409.42(10)	2.6(5)	$E2$	100(12)	1193.847(25)	2^{+}
				437.42(3)	100(5)	$E1$		1165.765(22)	1^{-}
				557.12(6)	10.4(18)[a]	$E2$	88(4)	1046.150(19)	2^{+}
				1269.32(8)	43.6(13)	$E2$	5.82(18)	333.926(18)	2^{+}

TABLE V. *(Continued.)*

NDS		Present work							
E (keV)	J^π	E_{level}	J^π	E_γ (keV)	I_γ	γ mult.	$B(E2)_{\text{rel}}$	E_{final}	J_f^π
1658.390(30)	$2^{(-)}$	1658.379(21)	2^-	153.75(20)	0.050(11)	$E1$		1504.574(29)	3^+
				241.08(18)	0.030(6)	$E1$		1417.366(21)	2^+
				464.49(6)	0.30(3)	$E1$		1193.847(25)	2^+
				492.65(4)	2.48(14)	$M1+E2$		1165.765(22)	1^-
				587.02(4)	8.7(4)	$M1+E2$		1071.421(26)	3^-
				612.18(4)	6.1(3)	$E1$		1046.150(19)	2^+
				1324.45(5)	100(5)	$E1$		333.926(18)	2^+
1684.162(17)	3^-	1684.29(6)	3^-	910.88(7)	54(4)	$E1$		773.37(4)	4^+
				1350.32(7)	100(7)	$E1$		333.926(18)	2^+
1713.51(5)	1	1713.25(3)	1^-	547.56(13)	1.12(9)	$M1+E2$		1165.765(22)	1^-
				667.13(5)	6.0(4)	$E1$		1046.150(19)	2^+
				972.77(8)	3.74(23)	$E1$		740.447(22)	0^+
				1379.30(5)	100(5)	$E1$		333.926(18)	2^+
				1713.19(11)	12.8(6)	$E1$		0	0^+
1786.30(13)	($\leqslant 3$)	1786.54(4)	0^+	369.03(12)	8.2(9)	$E2$	100(11)	1417.366(21)	2^+
				592.60(21)	1.3(4)	$E2$	1.5(4)	1193.847(25)	2^+
				620.76(3)	100(3)	$E1$		1165.765(22)	1^-
				740.44(6)	2.5(4)	$E2$	0.94(15)	1046.150(19)	2^+
				1452.68(8)	35(4)[a]	$E2$	0.475(15)	333.926(18)	2^+
1794.300(30)	2^+	1794.03(6)	2^+	600.30(10)	32(7)	$M1+E2$		1193.847(25)	2^+
				628.31(9)	100(10)	$E1$		1165.765(22)	1^-
				722.53(8)	32(13)[a]	$E1$		1071.421(26)	3^-
				747.87(7)	55(7)	$M1+E2$		1046.150(19)	2^+
				1053.52(8)	76(7)	$E2$		740.447(22)	0^+
				1460.3(4)	36(7)	$M1+E2$		333.926(18)	2^+
				1793.96(21)	32(5)	$E2$		0	0^+
1822.472(19)	$(3)^-$	1822.26(18)	4^-	1048.86(17)	100(10)	$E1$		773.37(4)	4^+
1833.010(30)	$(2)^+$	1833.52(6)	2^+	667.6(9)	35(7)	$E1$		1165.765(22)	1^-
				762.07(10)	42(4)	$E1$		1071.421(26)	3^-
				1059.98(18)	14.8(23)	$E2$	100(16)	773.37(4)	4^+
				1499.58(10)	100(14)	62% $E2$	74(27)	333.926(18)	2^+
				1833.64(16)	46(4)	$E2$	12(4)	0	0^+
1927.33(9)	(2^+)	1926.54(7)	2^+	242.2(3)	5.1(6)	$E1$		1684.29(6)	3^-
				760.79(9)	72(8)	$E1$		1165.765(22)	1^-
				855.08(12)	100(6)	$E1$		1071.421(26)	3^-
				1153.5(4)	18.6(19)	$E2$		773.37(4)	4^+
1952.460(30)	3^-	1950.83(9)	3^-	1177.44(8)	100(8)	$E1$		773.37(4)	4^+
				1616.3(5)	7.5(15)	$E1$		333.926(18)	2^+
1963.72(4)	$1^{(-)}$	1963.595(22)	1^-	250.45(20)	0.066(13)	$M1+E2$		1713.25(3)	1^-
				279.17(12)	0.08(3)[a]	$E2$		1684.29(6)	3^-
				305.16(10)	0.16(3)	$M1+E2$		1658.379(21)	2^-
				360.31(5)	1.09(15)[a]	$E1$		1603.24(4)	0^+
				546.19(14)	0.51(5)	$E1$		1417.366(21)	2^+
				707.90(9)	0.54(9)	$E1$		1255.480(25)	0^+
				769.76(9)	0.81(7)	$E1$		1193.847(25)	2^+
				797.88(21)	0.34(7)	$M1+E2$		1165.765(22)	1^-
				892.18(5)	1.46(11)	$E2$		1071.421(26)	3^-
				917.48(3)	22.9(6)	$E1$		1046.150(19)	2^+
				1223.13(5)	100(3)	$E1$		740.447(22)	0^+
				1629.68(5)	30.7(11)	$E1$		333.926(18)	2^+
				1963.60(5)	56(3)	$E1$		0	0^+
2005.5(8)	2^+	2004.40(7)	2^+	1263.95(16)	13.8(21)	$E2$	100(15)	740.447(22)	0^+
				1670.46(8)	100(6)	$M1+E2$	<180	333.926(18)	2^+
				2004.2(4)	3.8(12)	$E2$	2.8(9)	0	0^+

TABLE V. *(Continued.)*

NDS		Present work							
E (keV)	J^π	E_{level}	J^π	E_γ (keV)	I_γ	γ mult.	$B(E2)_{\text{rel}}$	E_{final}	J_f^π
2070.270(23)	$2^{(-)}$	2070.245(25)	2^-	237.1(8)	0.47(3)	$E1$		1833.52(6)	2^+
				276.35(4)	1.41(8)	$E1$		1794.03(6)	2^+
				356.93(8)	0.201(22)	$M1+E2$		1713.25(3)	1^-
				385.87(15)	0.052(7)	$M1+E2$		1684.29(6)	3^-
				411.89(12)	0.81(6)	$M1+E2$		1658.379(21)	2^-
				565.72(4)	19.1(10)	$E1$		1504.574(29)	3^+
				652.90(5)	4.82(26)	$E1$		1417.366(21)	2^+
				876.40(4)	100(5)	$E1$		1193.847(25)	2^+
				904.49(4)	12.4(7)	$M1+E2$		1165.765(22)	1^-
				998.76(9)	0.69(5)	$M1+E2$		1071.421(26)	3^-
				1024.01(4)	10.6(10)	$E1$		1046.150(19)	2^+
				1736.31(5)	78(7)	$E1$		333.926(18)	2^+
		2226.47(6)	(3^-)	1032.69(10)	25(4)	$E1$		1193.847(25)	2^+
				1061.1(4)	11(4)	$E2$		1165.765(22)	1^-
				1180.28(7)	100(6)	$E1$		1046.150(19)	2^+
2259.94(4)	(1^-)	2259.788(19)	1^-	426.27(16)	0.96(9)	$E1$		1833.52(6)	2^+
				546.50(23)	0.25(5)	$M1+E2$		1713.25(3)	1^-
				656.70(10)	1.00(18)	$E1$		1603.24(4)	0^+
				842.50(4)	48.2(26)	$E1$		1417.366(21)	2^+
				1004.23(4)	90(5)	$E1$		1255.480(25)	0^+
				1065.90(4)	45.3(27)	$E1$		1193.847(25)	2^+
				1093.94(15)	3.3(5)	$M1+E2$		1165.765(22)	1^-
				1188.54(17)	1.08(15)	$E2$		1071.421(26)	3^-
				1213.65(5)	100(5)	$E1$		1046.150(19)	2^+
				1519.34(6)	28.5(15)	$E1$		740.447(22)	0^+
				1925.88(6)	24.1(14)	$E1$		333.926(18)	2^+
				2259.78(14)	7.3(4)	$E1$		0	0^+
2367.43(8)	(3^+)	2367.398(40)	2^-	362.91(15)	0.30(22)	$E1$		2004.40(7)	2^+
				545.15(12)	1.9(4)	$E2$		1822.26(18)	4^-
				683.06(20)	0.68(13)	$M1+E2$		1684.29(6)	3^-
				709.13(20)	2.8(7)	$M1+E2$		1658.379(21)	2^-
				1173.67(10)	8.4(9)	$E1$		1193.847(25)	2^+
				1201.77(21)	3.0(6)	$M1+E2$		1165.765(22)	1^-
				1296.05(9)	6.5(5)	$M1+E2$		1071.421(26)	3^-
				2033.37(5)	100(5)	$E1$		333.926(18)	2^+
		2459.52(15)	$(1, 2^+)$	1413.37(16)	100(19)			1046.150(19)	2^+
				2459.5(4)	67(10)			0	0^+
2507.27(18)	$(1^{(-)}, 2^+)$	2507.79(6)	$1^{(-)}$	1090.68(20)	15(4)			1417.366(21)	2^+
				1461.7(3)	9(4)			1046.150(19)	2^+
				2173.81(7)	67(5)			333.926(18)	2^+
				2507.91(14)	100(6)			0	0^+
2529.40(30)	$1, 2^+$	2529.39(5)	(1^-)	871.06(20)	2.9(6)			1658.379(21)	2^-
				926.06(10)	3.2(5)			1603.24(4)	0^+
				1363.9(4)	3.1(7)			1165.765(22)	1^-
				1788.87(14)	5.4(5)			740.447(22)	0^+
				2195.41(6)	19.5(12)			333.926(18)	2^+
				2529.49(13)	100(5)			0	0^+
2550.57(23)	$1^{(-)}$	2550.56(6)	$(1, 2^+)$	837.58(20)	3.8(6)			1713.25(3)	1^-
				1133.02(23)	3.9(7)			1417.366(21)	2^+
				1295.02(22)	2.9(5)			1255.480(25)	0^+
				1504.6(3)	3.1(6)			1046.150(19)	2^+
				1810.05(10)	22.6(16)			740.447(22)	0^+
				2216.61(12)	100(6)			333.926(18)	2^+
				2550.51(15)	71(4)			0	0^+

TABLE V. *(Continued.)*

NDS		Present work							
E (keV)	J^π	E_{level}	J^π	E_γ (keV)	I_γ	γ mult.	$B(E2)_{\text{rel}}$	E_{final}	J_f^π
2602.5(4)	$(1^+, 2, 3)$	2602.29(5)	(2^-)	375.91(19)	2.8(7)			2226.47(6)	(3^-)
				532.07(20)	6.3(10)			2070.245(25)	2^-
				889.03(6)	55(3)			1713.25(3)	1^-
				1436.52(7)	100(7)			1165.765(22)	1^-
		2607.16(10)	$(1, 2^+)$	1413.2(3)	66(16)			1193.847(25)	2^+
				1561.27(18)	86(15)			1046.150(19)	2^+
				1866.63(22)	69(8)			740.447(22)	0^+
				2273.08(15)	100(12)			333.926(18)	2^+
				2607.2(5)	86(13)			0	0^+
		2705.06(7)	$(1, 2^+)$	740.5(3)	75(12)			1963.595(22)	1^-
				1101.77(16)	14(3)			1603.24(4)	0^+
				1448.7(3)	7.6(17)			1255.480(25)	0^+
				1964.63(11)	43(4)			740.447(22)	0^+
				2371.21(13)	100(6)			333.926(18)	2^+
2812.88(10)	$(1^-, 2)$	2812.96(3)	$(2,3^-)$	808.6(3)	4.6(9)			2004.40(7)	2^+
				862.11(9)	8.1(16)			1950.83(9)	3^-
				886.62(10)	16.2(15)			1926.54(7)	2^+
				990.4(3)	0.31(16)			1822.26(18)	4^-
				1128.60(11)	7.7(8)			1684.29(6)	3^-
				1154.57(5)	100(6)			1658.379(21)	2^-
				1308.4(4)	2.2(5)			1504.574(29)	3^+
				1647.17(7)	48(3)			1165.765(22)	1^-
				1741.53(16)	5.0(5)			1071.421(26)	3^-
				1766.78(9)	28.7(18)			1046.150(19)	2^+
				2479.03(13)	54(3)			333.926(18)	2^+
2893.10(30)	$(1^-, 2)$	2893.06(6)	(2^-)	633.03(15)	40.6(24)			2259.788(19)	1^-
				929.30(9)	19.3(19)			1963.595(22)	1^-
				1179.92(11)	13.2(12)			1713.25(3)	1^-
				1727.51(6)	100(7)			1165.765(22)	1^-
				2120.3(3)	1.2(4)			773.37(4)	4^+
		2895.19(10)	$(1, 2^+)$	968.83(13)	11.2(19)			1926.54(7)	2^+
				1210.3(8)	3.5(6)			1684.29(6)	3^-
				1849.09(21)	4.9(7)			1046.150(19)	2^+
				2154.3(3)	1.5(3)			740.447(22)	0^+
				2560.7(3)	4.1(5)			333.926(18)	2^+
				2895.3(3)	100(5)			0	0^+
		2936.05(8)	(1,2,3)	675.95(17)	65(9)			2259.788(19)	1^-
				1251.84(16)	50(7)			1684.29(6)	3^-
				1770.20(21)	77(10)			1165.765(22)	1^-
				1864.73(11)	100(9)			1071.421(26)	3^-
				2601.9(5)	12.9(23)			333.926(18)	2^+
		2987.15(5)	(1,2)	982.67(24)	28(3)			2004.40(7)	2^+
				1036.23(9)	18(3)			1950.83(9)	3^-
				1328.83(10)	100(8)			1658.379(21)	2^-
				1570.41(25)	4.2(11)			1417.366(21)	2^+
				1915.71(9)	50(4)			1071.421(26)	3^-
				1940.94(9)	12.6(15)			1046.150(19)	2^+
				2653.1(3)	8.8(10)			333.926(18)	2^+
		3025.53(17)	$(1, 2^+)$	2285.03(23)	36(5)			740.447(22)	0^+
				2691.6(3)	24(4)			333.926(18)	2^+
				3025.4(4)	100(6)			0	0^+
3038.2(4)	$1, 2^+$	3038.81(18)	$(1, 2^+)$	2704.84(19)	100(8)			333.926(18)	2^+
				3038.8(4)	58(4)			0	0^+
3050.00(30)	$1^{(-)}$	3050.56(20)	$(1, 2^+)$	2310.2(4)	25(6)			740.447(22)	0^+
				2716.56(26)	72(8)			333.926(18)	2^+

TABLE V. *(Continued.)*

NDS		Present work							
E (keV)	J^π	E_{level}	J^π	E_γ (keV)	I_γ	γ mult.	$B(E2)_{\text{rel}}$	E_{final}	J_f^π
				3050.5(4)	100(7)			0	0^+
		3071.46(6)	$\leqslant 3$	811.66(9)	57(11)			2259.788(19)	1^-
				1358.20(11)	73(6)			1713.25(3)	1^-
				1905.70(9)	100(11)			1165.765(22)	1^-
3080.9(4)	$1^{(+)}$	3082.21(27)	$(1, 2^+)$	2748.47(32)	28(5)			333.926(18)	2^+
				3081.6(5)	100(7)			0	0^+
		3093.85(21)	$(1, 2^+)$	2760.06(23)	42(8)			333.926(18)	2^+
				3093.0(5)	100(8)			0	0^+
3137.60(30)	(1, 2)	3139.50(10)	(2^+)	1455.37(30)	9(4)			1684.29(6)	3^-
				1634.85(21)	47(4)			1504.574(29)	3^+
				1973.57(21)	33.5(18)			1165.765(22)	1^-
				2067.59(30)	23(9)			1071.421(26)	3^-
				2805.76(18)	100(5)			333.926(18)	2^+
				3140.1(6)	12(8)			0	0^+
		3191.63(23)	$(1, 2^+)$	2857.74(24)	100(15)			333.926(18)	2^+
			$(1, 2^+)$	3191.1(6)	40(6)			0	0^+

[a]Normalized residuals method used to determine the value and uncertainty of the combined relative γ intensity for these somewhat discrepant data.

somewhat discrepant intensity data, the normalized residual method was used, and identified as such on the table. These procedures were carried out following the methods in the V.AveLib software package [32].

[1] E. Ganioglu, R. Wyss, and P. Magierski, Phys. Rev. C **89**, 014311 (2014).
[2] S. P. Bvumbi *et al.*, Phys. Rev. C **87**, 044333 (2013).
[3] H. Mach, M. Hellström, B. Fogelberg, D. Jerrestam, and L. Spanier, Phys. Rev. C **46**, 1849 (1992).
[4] M. Babilon, N. V. Zamfir, D. Kusnezov, E. A. McCutchan, and A. Zilges, Phys. Rev. C **72**, 064302 (2005).
[5] A. Chakraborty, F. M. Prados-Estévez, S. N. Choudry, B. P. Crider, P. E. Garrett, W. D. Kulp, A. Kumar, M. T. McEllistrem, S. Mukhopadhyay, M. G. Mynk, J. N. Orce, E. E. Peters, J. L. Wood, and S. W. Yates, Phys. Rev. C **86**, 064314 (2012).
[6] P. E. Garrett, W. D. Kulp, J. L. Wood, D. Bandyopadhyay, S. Choudry, D. Dashdorj, S. R. Lesher, M. T. McEllistrem, M. Mynk, J. N. Orce, and S. W. Yates, Phys. Rev. Lett. **103**, 062501 (2009).
[7] M. F. Kidd, J. H. Esterline, S. W. Finch, and W. Tornow, Phys. Rev. C **90**, 055501 (2014).
[8] A. S. Barabash, P. Hubert, A. Nachab, and V. I. Umatov, Phys. Rev. C **79**, 045501 (2009).
[9] M. Hoshi, M. Fujiwara, and Y. Yoshizawa, J. Phys. Soc. Jpn. **42**, 1098 (1977).
[10] M. Hoshi, T. Shimoshige, and Y. Yoshizawa, J. Phys. Soc. Jpn. **42**, 1091 (1977).
[11] J. Barrette, M. Barrette, S. Monaro, S. Santhanam, and S. Markiza, Can. J. Phys. **48**, 1161 (1970).
[12] P. Humby, A. Simon, C. W. Beausang, J. M. Allmond, J. T. Burke, R. J. Casperson, R. Chyzh, M. Dag, K. Gell, R. O. Hughes, J. Koglin, E. McCleskey, M. McCleskey, S. Ota, T. J. Ross, A. Saastamoinen, T. Tarlow, and G. Vyas, Phys. Rev. C **94**, 064314 (2016).
[13] H. G. Börner, P. Mutti, M. Jentschel, N. V. Zamfir, R. F. Casten, E. A. McCutchan, and R. Krücken, Phys. Rev. C **73**, 034314 (2006).
[14] A. Passoja, J. Kantele, M. Luontama, R. Julin, E. Hammaren, P. Lipas, and P. Toivonen, J. Phys. G **12**, 1047 (1986).
[15] D. J. Buss and R. K. Smither, Phys. Rev. C **2**, 1513 (1970).
[16] J. Martin, D. Radford, M. Beaulieu, P. Taras, D. Ward, H. Andrews, G. Ayotte, F. Sharp, J. Waddington, O. Häusser *et al.*, Nucl. Instrum. Methods Phys. Res., Sect. A **257**, 301 (1987).
[17] D. Radford, Radware data analysis software (v05.3), 2011.
[18] S. K. Basu and A. A. Sonzogni, Nucl. Data Sheets **114**, 435 (2013); see also Evaluated Nucelar Structure Data File, www.nndc.bnl/ensdf.
[19] J. Gupta, K. Kumar, and J. Hamilton, Int. J. Mod. Phys. E **19**, 1491 (2010).
[20] J. Wood, K. Heyde, W. Nazarewicz, M. Huyse, and P. Van Duppen, Phys. Rep. **215**, 101 (1992).
[21] J. Wood, E. Zganjar, C. De Coster, and K. Heyde, Nucl. Phys. A **651**, 323 (1999).
[22] N. Stone, At. Data Nucl. Data Tables **111-112**, 1 (2016).
[23] W. Kulp, J. L. Wood, P. E. Garrett, C. Y. Wu, D. Cline, J. M. Allmond, D. Bandyopadhyay, D. Dashdorj, S. N. Choudry, A. B. Hayes *et al.*, arXiv:0706.4129.
[24] P. Garrett and J. Wood, J. Phys. G: Nucl. Part. Phys. **37**, 064028 (2010).
[25] W. Kulp, J. Wood, P. Garrett, C. Wu, D. Cline, J. Allmond, D. Bandyopadhyay, D. Dashdorj, S. Choudry, A. Hayes *et al.*, Phys. Rev. C **77**, 061301 (2008).

[26] J. Sharpey-Schafer, S. Mullins, R. Bark, J. Kau, F. Komati, E. Lawrie, J. Lawrie, T. Madiba, P. Maine, A. Minkova *et al.*, Eur. Phys. J. A **47**, 5 (2011).
[27] P. Garrett, J. Wood, and S. Yates, Phys. Scr. **93**, 063001 (2018).
[28] K. Heyde and J. L. Wood, Rev. Mod. Phys. **83**, 1467 (2011).
[29] W. Kulp, Phys. Rev. Lett. **91**, 102501 (2003).
[30] W. Kulp, J. Wood, P. Garrett, J. Allmond, D. Cline, A. Hayes, H. Hua, K. Krane, R.-M. Larimer, J. Loats *et al.*, Phys. Rev. C **71**, 041303 (2005).
[31] I. Ragnarsson and R. Broglia, Nucl. Phys. A **263**, 315 (1976).
[32] M. Birch, Visual averaging library (v1.2.2), 2016.